



**HAL**  
open science

# Stochastic inversion of permeability and dispersivities from time lapse self-potential measurements: A controlled sandbox study

A. Revil, Abderrahim Jardani

► **To cite this version:**

A. Revil, Abderrahim Jardani. Stochastic inversion of permeability and dispersivities from time lapse self-potential measurements: A controlled sandbox study. *Geophysical Research Letters*, 2010, 37, pp.11404. 10.1029/2010GL043257 . insu-00565058

**HAL Id: insu-00565058**

**<https://insu.hal.science/insu-00565058>**

Submitted on 10 Mar 2021

**HAL** is a multi-disciplinary open access archive for the deposit and dissemination of scientific research documents, whether they are published or not. The documents may come from teaching and research institutions in France or abroad, or from public or private research centers.

L'archive ouverte pluridisciplinaire **HAL**, est destinée au dépôt et à la diffusion de documents scientifiques de niveau recherche, publiés ou non, émanant des établissements d'enseignement et de recherche français ou étrangers, des laboratoires publics ou privés.

# Stochastic inversion of permeability and dispersivities from time lapse self-potential measurements: A controlled sandbox study

A. Revil<sup>1,2</sup> and A. Jardani<sup>3</sup>

Received 14 March 2010; revised 23 April 2010; accepted 28 April 2010; published 8 June 2010.

[1] We test the ability of the self-potential method to provide information that can be used to invert the permeability and the dispersivities of a porous material. We first formulate the semi-coupled system of equations describing the occurrence of self-potential signals associated with the transport of salt in a porous material like sand. Two contributions in the source current density arise from the electrokinetic coupling associated with the flow of the pore water and the diffusion potential due to the gradient in the activity of the salt. A controlled laboratory sandbox experiment is performed to show that time-lapse self-potential measurements can be used to invert, in a Bayesian framework, the permeability and dispersivities. **Citation:** Revil, A., and A. Jardani (2010), Stochastic inversion of permeability and dispersivities from time lapse self-potential measurements: A controlled sandbox study, *Geophys. Res. Lett.*, *37*, L11404, doi:10.1029/2010GL043257.

## 1. Introduction

[2] Imaging aquifer transport properties is an important task in hydrogeophysics. The non-intrusive monitoring of salt plume is traditionally done using GPR or electrical resistivity tomography with the goal of inferring the distribution of the permeability and dispersivities. In this letter, we are looking for a passive (real-time) monitoring and non-intrusive geophysical method to monitor a salt tracer test. The expression “non-intrusive” is used below to say that we measure remotely the geophysical signal generated by the presence of a plume of salt water. In our approach, the presence of a salt plume generates indeed an electrical current on its own and this electrical current generates in turn an electrical field called the self-potential field. *Maineult et al.* [2005] showed that the migration of a salt plume creates an electrical field that can be explained by combining electrokinetic and diffusion potential theories. However they put their electrodes directly in contact with the salt plume, so their measurements were intrusive. While this was a good start, we feel that the self-potential method can be used remotely to investigate the plume properties over time.

## 2. Background Theory

[3] The constitutive equations are Darcy’s law for the Darcy velocity  $\mathbf{u}$  (in  $\text{m s}^{-1}$ ), Fick’s law for the flux of the salt

$\mathbf{j}_d$  (in  $\text{kg m}^{-2} \text{s}^{-1}$ ), and Ohm’s law for the current density  $\mathbf{j}$  (in  $\text{A m}^{-2}$ ),

$$\mathbf{u} = \phi \mathbf{v} = -\frac{1}{\eta_f} \mathbf{k} \cdot (\nabla p + \rho_f g \nabla z), \quad (1)$$

$$\mathbf{j}_d = -\rho_f \phi \mathbf{D} \cdot \nabla C_m + \rho_f \phi \mathbf{v} C_m, \quad (2)$$

$$\mathbf{j} = -\sigma \cdot \nabla \varphi + \bar{Q}_V \mathbf{u} - k_b T \sum_{i=1}^N \frac{T_i}{q_i} \sigma \cdot \nabla \ln \{i\}, \quad (3)$$

(see *Oltean and Buès* [2002] for equations (1) and (2) and *Revil and Linde* [2006] for equation (3)) where  $\mathbf{v}$  is the mean velocity of the pore water ( $\text{m s}^{-1}$ ),  $\mathbf{k}$  (in  $\text{m}^2$ ) is the permeability tensor,  $\mathbf{D}$  (in  $\text{m}^2 \text{s}^{-1}$ ) is the hydrodynamic dispersion tensor,  $\sigma = \sigma \mathbf{I}_3$  is the electrical conductivity tensor (in  $\text{S m}^{-1}$ ),  $\mathbf{I}_3$  is the  $3 \times 3$  unit tensor,  $\phi$  [–] is the connected porosity,  $p$  is the pore pressure (Pa),  $\varphi$  is the self-potential (in V),  $C_m$  is the solute mass fraction (dimensionless),  $\eta_f$  is the dynamic viscosity of the fluid (in Pa s),  $\rho_f$  is the solute bulk density (in  $\text{kg m}^{-3}$ ),  $g = 9.81 \text{ m s}^{-2}$ ,  $k_b$  is the Boltzmann constant ( $1.381 \times 10^{-23} \text{ J K}^{-1}$ ),  $q_i$  is the charge (in C) of species  $i$  dissolved in water  $\{i\}$  is the activity of species  $i$ ,  $T_i$  (dimensionless) is the macroscopic Hittorf number of the ionic species  $i$  in the porous material (that is the fraction of electrical current carried by species  $i$ ), and  $\{i\}$  (in  $\text{m}^{-3}$ ) represents the activity of the ionic species  $i$ , and  $\bar{Q}_V$  (in  $\text{C m}^{-3}$ ) is the excess charge density (due to the diffuse layer) of the pore water per unit pore volume. The charge density  $\bar{Q}_V$  can be predicted from permeability according to  $\log_{10} \bar{Q}_V = -9.2 - 0.82 \log_{10} k$  [*Jardani and Revil*, 2009].

[4] In addition to the constitutive equations, we have to consider three continuity equations for the mass of the pore water, for the mass of the salt, and for the electrical charge,

$$\nabla \cdot (\rho_f \mathbf{u}) = -\frac{\partial(\rho_f \phi)}{\partial t} + \rho_f Q_S \quad (4)$$

$$\nabla \cdot \mathbf{j}_d = -\frac{\partial(\rho_f \phi C_m)}{\partial t} + \rho_f Q_S C_m^0, \quad (5)$$

$$\nabla \cdot \mathbf{j} = 0, \quad (6)$$

where  $C_m^0$  is the solute mass fraction of the salt in the source term,  $Q_S$  is a volumetric hydraulic source term for the injection/abstraction of water (in  $\text{s}^{-1}$ ). The effect of the salt concentration on the mass density and viscosity are given by *Oltean and Buès* [2002]:  $\rho_f = \rho_f^0 + \gamma C_m$  and  $\eta_f = \eta_f^0 (1 + \tau_1 C_m + \tau_2 C_m^2 + \tau_3 C_m^3)$ , where  $\rho_f^0$  and  $\eta_f^0$  are the mass density and viscosity of pure water, respectively,  $\gamma$ ,  $\tau_1$ ,  $\tau_2$ ,  $\tau_3$  are empirical constants.

<sup>1</sup>Department of Geophysics, Colorado School of Mines, Golden, Colorado, USA.

<sup>2</sup>Equipe Volcan, LGIT, UMR 5559, Université de Savoie, CNRS, Le Bourget-du-Lac, France.

<sup>3</sup>M2C, UMR 6143, Université de Rouen, CNRS, Mont-Saint-Aignan, France.

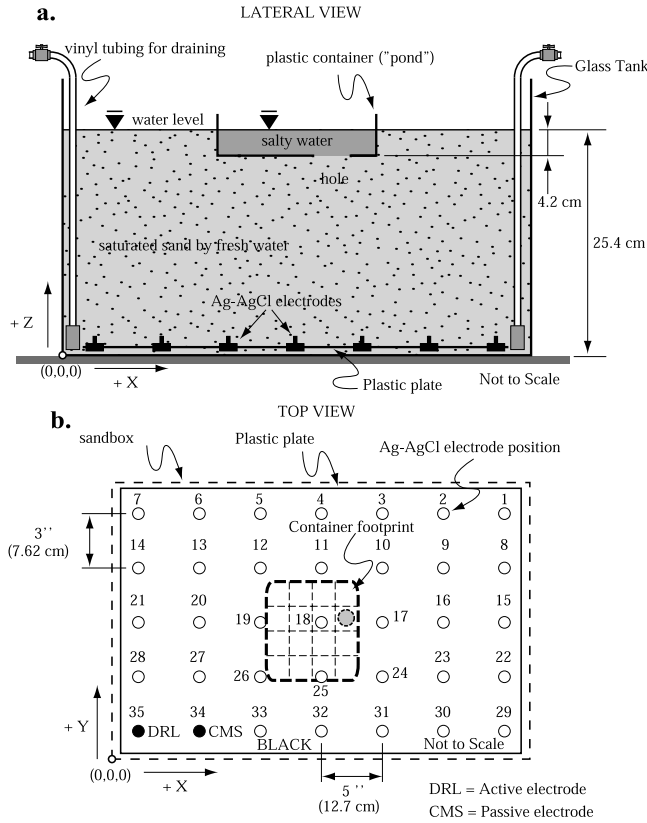


**Figure 1.** Sketch of the experimental setup. (a) Side view. (b) Top view with the position of the electrodes. CMS is the reference for the self-potential network of electrodes. The salt plume is sinking from the hole at the bottom of the container into the sandbox.

[5] Neglecting the effect of surface conductivity, the conductivity of the sand is,

$$\sigma = \frac{\sigma_f}{F}, \quad (7)$$

where  $F = \phi^{-m}$  [-] is the electrical formation factor,  $\sigma_f$  is the pore water conductivity, and  $m$  [-] is the cementation exponent. The effect of the salinity upon the electrical conductivity is accounted for by using *Sen and Goode's* [1992] model, which is valid from dilute concentrations to saturation in salt.

[6] In the widely used Fickian model, the hydrodynamic dispersion tensor is given by

$$\mathbf{D} = \left[ \frac{D_m}{\alpha} + \alpha_T v \right] \mathbf{I}_3 + \frac{\alpha_L - \alpha_T}{v} \mathbf{v} \otimes \mathbf{v}, \quad (8)$$

where  $D_m$  is the molecular (mutual) diffusion coefficient of the salt (in  $\text{m}^2 \text{s}^{-1}$ ) (for a NaCl solution,  $D_m$  is  $\sim 1.60 \times 10^{-9} \text{ m}^2 \text{ s}^{-1}$  at infinite dilution and  $\sim 1.44 \times 10^{-9} \text{ m}^2 \text{ s}^{-1}$  at high salinities at  $25^\circ\text{C}$ ),  $v = |\mathbf{v}|$ ,  $\mathbf{a} \otimes \mathbf{b}$  represents the tensorial product between vectors  $\mathbf{a}$  and  $\mathbf{b}$ , and  $\alpha_L$  and  $\alpha_T$  are the longitudinal (along  $\mathbf{v}$ ) and transverse (normal to  $\mathbf{v}$ ) dispersivities (in m),

and  $\alpha$  is the tortuosity. A generalization of equation (8) to anisotropic media is given by *Neuman et al.* [1987].

### 3. Forward and Inverse Modeling

[7] The forward modeling of the field equations obtained by combining equations (1) to (6) and the additional relationships for the material properties can be done with the finite element solver Comsol Multiphysics 3.4. We first solve the coupled hydrodynamic equations including the buoyancy effect. Then the solution is used to solve for the divergence of the source current density in the electrostatic Poisson equation,

$$\nabla \cdot (\sigma \nabla \phi) = \nabla \cdot \mathbf{j}_S, \quad (9)$$

$$\mathbf{j}_S = \bar{Q}_V \mathbf{u} - \frac{k_b T}{F e} (2t_{(+)} - 1) \nabla \sigma_f, \quad (10)$$

where  $t_{(+)} = 0.38$  (NaCl) is the microscopic Hittorf number of the cations in the pore water. Equation (10) is obtained using the approach outlined by *Revil* [1999].

[8] We are looking for an algorithm to invert  $\mathbf{k}$  and  $\mathbf{D}$  accounting for the resistivity distribution, which change over time, and the possible non-uniqueness of the inverse problem. We use below a variant of the Markov chain Monte Carlo methods called the Adaptive Metropolis Algorithm (AMA) [*Haario et al.*, 2001]. This algorithm is based on the traditional Metropolis algorithm with a symmetric Gaussian proposal distribution centered at the current model  $\mathbf{m}^i$  and with the covariance  $\mathbf{C}^i$  that changes during the sampling in such a way that the sampling efficiency increases over time. Recent applications of the AMA algorithm are given by *Jardani and Revil* [2009] for the joint inversion of temperature and self-potential data.

### 4. Experiment and Inversion

[9] We performed a sandbox experiment to invert the time-lapse self-potential response resulting from the leakage of salty water from a small tank into a sandbox (Figure 1). The sandbox was filled with a well-sorted silica sand with a measured porosity of 0.40, a measured cementation exponent  $m = 1.5$ , and a median grain diameter  $d_{50} = 350 \mu\text{m}$ . The sandbox was initially saturated with tap water with  $\sigma_f = (1.5 \pm 0.2) \times 10^{-3} \text{ S m}^{-1}$ . We can check that surface conductivity can be neglected as the ratio of surface to bulk conductivity  $\text{Du} = 4 \Sigma_s / d_{50} \sigma_f = 5 \times 10^{-2} \ll 1$  where  $\Sigma_s(25^\circ\text{C}) = 4 \times 10^{-9} \text{ S}$  is the specific surface conductance.

[10] On the top of the saturated sand surface, we setup a small plastic container with an impervious and insulating (plastic) boundary (Figure 1). This container was filled with salty water (NaCl,  $\sim 5.5 \text{ Mol/L}$ ,  $\sigma_f = 34.5 \text{ S m}^{-1}$  at  $20^\circ\text{C}$ ). The level of water was the same in the container and in the sandbox. On the bottom of the container, a hole was made with a diameter of 1.25 cm (Figure 1). The hole was initially sealed with a sticky tape before starting the measurements. Prior to removing the tape, the self-potential signals were recorded over 193 s (Figure 2). In this phase (termed Phase I below), all of channels had values  $0.0 \pm 0.2 \text{ mV}$ . The second measurement phase (Phase II) started with the opening of the hole by removing quickly the sticky tape. This resulted in the formation of a salty plume sinking in the tank. At the start

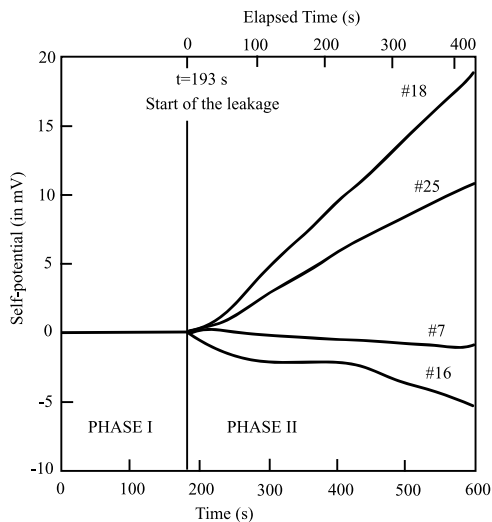


**Figure 2.** Display of the electrical potentials versus time for some selected electrodes (electrodes # 7, 16, 18, and 25), see position Figure 1 located at the bottom of the sandbox.

of Phase II, all the channels showed a significant and progressive change in their self-potential values (Figure 2). The highest changes were recorded approximately below the position of the hole (see Figure 3). Figure 3 shows maps of the self-potential distributions at total times 211 s, 303 s, 382 s, and 421 s (the leakage starts at  $t = 193$  s). The experiment was run at  $21^{\circ}\text{C}$ .

[11] A network of 34 sintered 1 mm Ag/AgCl electrodes was located at the bottom of the sandbox (Figure 1). The electrodes were connected to a precision digital Biosemi voltmeter having a capacity of 256 sensor-signals digitized

with 24 bit resolution. Each channel consists of a low noise DC coupled post-amplifier, with a first order anti-aliasing filter, followed by a 24 bit Delta-Sigma modulator based analog to digital (AD) converter having an oversampling rate of 64, achieved with a post modulator decimation filter. The digital output of all the AD converters are digitally multiplexed into a serial data stream and sent to a PC via a single optical fiber through a fiber to USB interface. This voltmeter has a resolution of  $\sim 0.1 \mu\text{V}$  (amplification of 32), a bandwidth from DC to 400 Hz, with an input impedance for the electrodes of 300 Mohm at 50 Hz [Haas and Revil, 2009].

[12] We use a 128 Hz acquisition sampling and later the data were further decimated in Matlab to a final decimated sample rate of 32 Hz. Because the data acquisition system was designed to have a broad dynamic range, electronic circuits were designed into it to minimize the effects of common mode signals appearing at the electrode inputs. These circuits employ 2 electrodes, the Common Mode Sense (CMS) and Dynamic Reference Level (DRL) electrodes. These electrodes are used together in a feedback loop to keep the potential of the sand close to the reference level of the AD converters used in the system. All electrode voltages measured are referenced to the CMS electrode. The DRL electrode is the only driven electrode in the measurement system and provides the signal return path for all of the electrodes with a current limit of  $50 \mu\text{A}$ . These 2 electrodes form a dynamic reference level circuit that is used in the system to improve common mode voltage rejection.

[13] Forward modeling was performed with an open boundary at the top of the sandbox (except at the position of the small tank) and impervious boundaries elsewhere. The mass density of salt water at saturation is  $\rho_S = 1202 \text{ kg m}^{-3}$ . The head at the bottom of the container is therefore  $\rho_S g \delta h = 495 \text{ Pa}$  with  $\delta h = 4.2 \text{ cm}$ . At the same depth the head in the

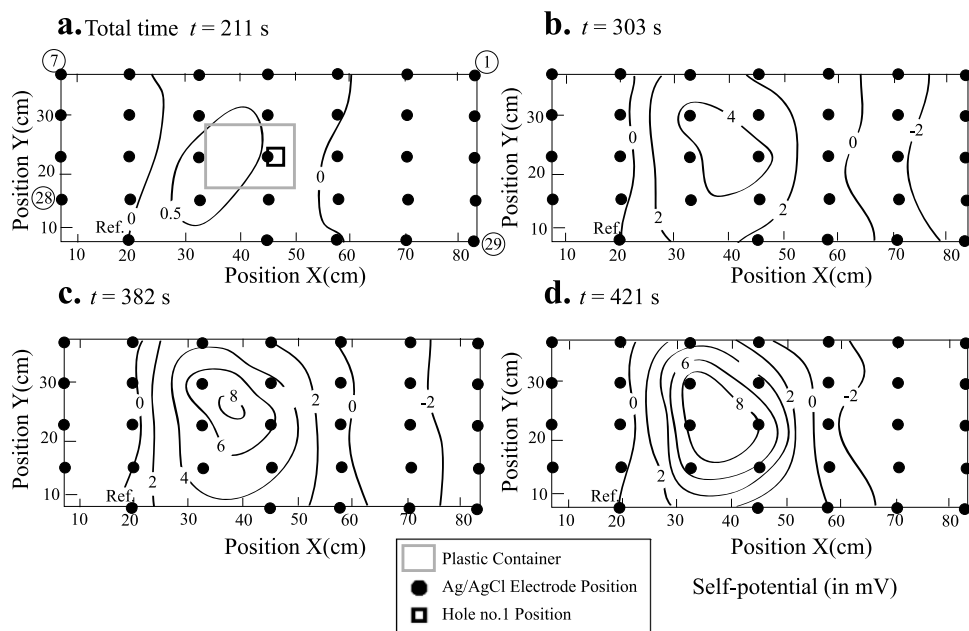


**Figure 3.** Self-potential maps at the bottom of the tank versus time at four different total times following the start of the leak at  $t = 193$  s (Phase II). The distribution before  $t = 193$  s is zero everywhere with an uncertainty of 0.2 mV. “Ref” indicates the position of the reference electrode (0 mV).

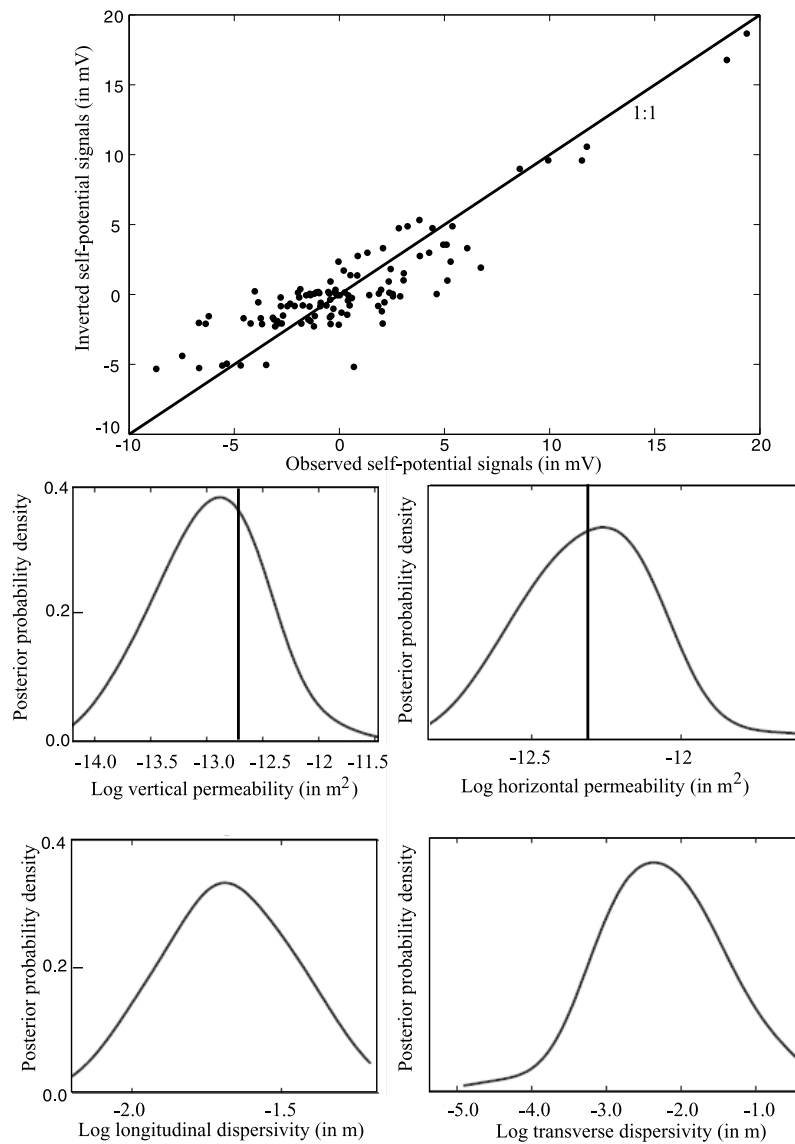


**Figure 4.** Posterior probability densities for the four model parameters and quality of the fit of the self-potential data using the most likely values of the four model parameters (RMS = 0.79). The model parameters include the two components of the permeability tensor and the transverse and longitudinal dispersivities. The vertical bars correspond to the measured vertical and horizontal permeabilities.

sandbox is  $\rho_w g \delta h = 412$  Pa with  $\rho_w = 1000$  kg m<sup>-3</sup>. Therefore there is an excess head in the reservoir of 83 Pa, which represents an excess of head of 0.85 cm of fresh water. Knowing the size of the leaking area (a hole with a diameter of 1.25 cm),  $Q_S$  can be easily computed as a function of time. All the external boundaries are insulating.

[14] We consider that because the sand has angular grains, compaction of the sand in the sandbox is responsible for a vertical transversely isotropic material with the horizontal plane as the symmetry plane. Therefore in a Cartesian coordinate system with  $z$  the vertical axis, the permeability tensor is given by

$$\mathbf{k} = \begin{bmatrix} k_x & 0 & 0 \\ 0 & k_x & 0 \\ 0 & 0 & k_z \end{bmatrix}. \quad (11)$$

[15] The model vector is  $\mathbf{m} = (\log k_x, \log k_z, \log \alpha_T, \log \alpha_L)$  to ensure the positiveness of the four material properties. The likelihood function used to assess for the quality of a model  $\mathbf{m}$  is:

$$P(\mathbf{d}|\mathbf{m}) = \frac{1}{[(2\pi)^N \det \mathbf{C}_d]^{1/2}} \exp \left[ -\frac{1}{2} (\mathbf{g}(\mathbf{m}) - \mathbf{d})^T \mathbf{C}_d^{-1} (\mathbf{g}(\mathbf{m}) - \mathbf{d}) \right] \quad (12)$$

where  $\mathbf{g}(\mathbf{m})$  is the forward modeling operator for the chemiohydroelectrical problem. It connects the generation of a self-potential anomaly to a variation of the material properties,  $\mathbf{d}$  is a  $N$ -vector of the observed self-potential data at different time intervals. The  $(N \times N)$ -covariance matrix  $\mathbf{C}_d$  is a diagonal matrix determined using the standard deviations on the measurements (1 mV). We use the AMA algorithm to explore the posterior probability density  $\pi(\mathbf{m}|\mathbf{d})$

of the model parameters  $\mathbf{m}$  given the data  $\mathbf{d}$ ,  $\pi(\mathbf{m}|\mathbf{d}) \propto P(\mathbf{d}|\mathbf{m})P_0(\mathbf{m})$  with  $P_0(\mathbf{m})$  the prior probability density or belief on model parameters  $\mathbf{m}$  also taken Gaussian distributed. The Bayesian solution of the inverse problem is the whole posterior probability distribution of the material properties. Let us assume that we have sampled the states  $(\mathbf{m}^0, \dots, \mathbf{m}^{i-1})$  where  $\mathbf{m}^0$  corresponds to the initial state. Then a candidate point  $\mathbf{m}'$  is sampled from the Gaussian proposal distribution  $q$  with mean point at the present point  $\mathbf{m}^{i-1}$  and with the covariance:

$$\mathbf{C}^i = \begin{cases} \mathbf{C}^0 & \text{if } i \leq n_0 \\ s_n \mathbf{K}^i + s_n \varepsilon \mathbf{I}_n & \text{if } i > n_0 \end{cases}, \quad (13)$$

where  $\mathbf{I}_n$  denotes the  $n$ -dimensional identity matrix,  $n_0 = 4$  model parameters,  $\varepsilon = 10^{-16}$ ,  $\mathbf{K}^i = \text{Cov}(\mathbf{m}^0, \dots, \mathbf{m}^{i-1})$  is the regularization factor (a small positive number that prevents the covariance matrix from becoming singular),  $\mathbf{C}^0$  is the initial covariance matrix,  $s_n = (2.4)^2/n$  is a parameter that depends only on the dimension of the vector  $\mathbf{m} \in \mathcal{R}^n$  [Gelman *et al.*, 1996]. The candidate realization  $\mathbf{m}'$  is accepted with the acceptance probability:

$$\alpha(\mathbf{m}^{i-1}; \mathbf{m}') = \min \left[ 1, \frac{\pi(\mathbf{m}'|\mathbf{d})}{\pi(\mathbf{m}^{i-1}|\mathbf{d})} \right]. \quad (14)$$

[16] If the candidate realization is accepted, we consider  $\mathbf{m}^i = \mathbf{m}'$ , otherwise  $\mathbf{m}^i = \mathbf{m}^{i-1}$ . The AMA algorithm was used to generate 10,000 realizations. We use the self-potential maps at the following times only: 211, 303, 421, and 600 s. We use the constraints:  $\log(k_x, k_z) \in [-11; -14]$  and  $\log(\alpha_T, \alpha_L) \in [-5; 0.5]$  with a uniform prior distribution on these intervals. After convergence, the statistics on the distribution of the model parameters are described by their posterior probability densities determined using the last 3000 realizations (Figure 4).

[17] The mean values of the inverted horizontal permeability agree well with the measured value in a sand permeameter ( $\log k_x = -12.3$ ). The vertical permeability is found to be smaller in agreement with an independently measured value ( $\log k_z = -12.7$ ). The result of the inversion for the longitudinal and transverse dispersivities are  $\log \alpha_L = -1.7 \pm 0.5$  and  $\log \alpha_T = -2.3 \pm 1.0$ . This is fairly consistent with the value reported by Sato *et al.* [2003] with  $\log \alpha_L$  between  $-2.5$  and  $-2.7$  for glass bead with  $d_{50} = 300 \mu\text{m}$ . In unconsolidated sands, the dispersivity can be described as  $\mathbf{D} = \mathbf{D}\mathbf{I}_3$  with  $D/D_m = 1/\alpha + 0.5 \text{ Pe}^{1.2}$  [Pfannkuch, 1963; Maineult *et al.*, 2005] where  $\alpha$  is the tortuosity of the pore space ( $\alpha = F \phi = 1.6$ ) and  $\text{Pe} = d_{50} v/D_m$  is the Peclet number. The velocity  $v$  of the front can be determined by the time taken by the salt plume to go from the small container to the electrodes (a strong electrical effect is created when the salt reached the electrode #18 at 1308 s). This time lapse is 1115 s. As the traveled distance is 21 cm, the velocity is therefore  $v = 1.9 \times 10^{-4} \text{ m s}^{-1}$ . Using  $d_{50} = 350 \mu\text{m}$ , we get  $\text{Pe} = 46$  and a dispersivity  $D \sim 7 \times 10^{-8} \text{ m}^2 \text{ s}^{-1}$ . The dispersivity can be compared with the inverted result using the self-potential

data:  $\alpha_L v = 4 \times 10^{-6} \text{ m}^2 \text{ s}^{-1}$ . Therefore, our estimates are fairly consistent with the properties of the sand.

## 5. Conclusions

[18] This is the first time that time-lapse self-potential monitoring is used to invert the permeability and effective dispersivities of a porous material. The advantages of the Bayesian approach coupled with a MCMC solver are: (1) it accounts for the possible non-uniqueness in the solution of the inverse problem, (2) electrical resistivity changes over time is automatically accounted for, (3) the geometry of the sandbox and boundary conditions are accounted for. While we have dealt with an homogeneous sandbox, the present approach can be used for heterogeneous field. Such a task would be however difficult if the only source of information is self-potential because of the low resolution of potential field methods. It would be complementary to complex resistivity time-lapse measurements. In addition, the measured signals are very small so the application of this method in the field would require a very sensitive equipment and a correction of the temperature drift of the electrodes.

[19] **Acknowledgments.** A. Revil thanks P. Martínez-Pagán, the Office of Science (BER), U.S. Department of Energy, grant DE-FG02-08ER646559 "Advanced self-potential tomography." A. Jardani thanks Seine Aval program for the project "TidHydrex". F. Day-Lewis and A. Binley are thanked for their very constructive reviews.

## References

- Gelman, A. G., G. O. Roberts, and W. R. Gilks (1996), Efficient metropolis jumping rules, in *Bayesian Statistics V*, edited by J. M. Bernardo *et al.*, pp. 599–608, Oxford Univ. Press, New York.
- Haas, A., and A. Revil (2009), Electrical signature of pore scale displacements, *Water Resour. Res.*, *45*, W10202, doi:10.1029/2009WR008160.
- Jardani, A., and A. Revil (2009), Stochastic joint inversion of temperature and self-potential data, *Geophys. J. Int.*, *179*(1), 640–654, doi:10.1111/j.1365-246X.2009.04295.x.
- Maineult, A., Y. Bernabé, and P. Ackerer (2005), Detection of advected concentration and pH fronts from spontaneous potential measurements, *J. Geophys. Res.*, *110*, B11205, doi:10.1029/2005JB003824.
- Neuman, S. P., C. L. Winter, and C. M. Newman (1987), Stochastic theory of field scale Fickian dispersion in anisotropic porous media, *Water Resour. Res.*, *23*(3), 453–466, doi:10.1029/WR023i003p00453.
- Oltean, C., and M. A. Buès (2002), Infiltration of salt solute in homogeneous and saturated porous Media—An analytical solution evaluated by numerical simulations, *Transp. Porous Media*, *48*, 61–78, doi:10.1023/A:1015628216337.
- Pfannkuch, H. O. (1963), Contribution à l'étude des déplacements de fluides miscibles dans un milieu poreux, *Rev. Inst. Fr. Pet.*, *18*(2), 215–270.
- Revil, A. (1999), Ionic diffusivity, electrical conductivity, membrane and thermoelectric potentials in colloids and granular porous media: A unified model, *J. Colloid Interface Sci.*, *212*, 503–522, doi:10.1006/jcis.1998.6077.
- Revil, A., and N. Linde (2006), Chemico-electromechanical coupling in microporous media, *J. Colloid Interface Sci.*, *302*, 682–694, doi:10.1016/j.jcis.2006.06.051.
- Sato, T., H. Tanakashi, and H. A. Loaiciga (2003), Solute dispersion in a variably saturated sand, *Water Resour. Res.*, *39*(6), 1155, doi:10.1029/2002WR001649.
- Sen, P. N., and P. A. Goode (1992), Influence of temperature on electrical conductivity on shaly sands, *Geophysics*, *57*, 89–96, doi:10.1190/1.1443191.
- A. Jardani, M2C, UMR 6143, Université de Rouen, CNRS, F-76821 Mont-Saint-Aignan CEDEX, France.
- A. Revil, Department of Geophysics, Colorado School of Mines, 1500 Illinois St., Golden, CO 80401, USA. (arevil@mines.edu)